

Hadron-Quark Crossover and Massive Hybrid Stars

Kota Masuda^{1,2,*}, Tetsuo Hatsuda², and Tatsuyuki Takatsuka^{3†}

¹*Department of Physics, The University of Tokyo, Tokyo 113-0033, Japan*

²*Theoretical Research Division, Nishina Center, RIKEN, Wako 351-0198, Japan*

³*Iwate University, Morioka 020-8550, Japan*

*E-mail: masuda@nt.phys.s.u-tokyo.ac.jp

.....
On the basis of the percolation picture from the hadronic phase with hyperons to the quark phase with strangeness, we construct a new equation of state (EOS) with the pressure interpolated as a function of the baryon density. The maximum mass of neutron stars can exceed $2M_{\odot}$ if the following two conditions are satisfied; (i) the crossover from the hadronic matter to the quark matter takes place at around three times the normal nuclear matter density, and (ii) the quark matter is strongly interacting in the crossover region. This is in contrast to the conventional approach assuming the first order phase transition in which the EOS becomes always soft due to the presence of the quark matter at high density. Although the choice of the hadronic EOS does not affect the above conclusion on the maximum mass, the three-body force among nucleons and hyperons plays an essential role for the onset of the hyperon mixing and the cooling of neutron stars.
.....

Subject Index Neutron stars, Nuclear matter aspects in nuclear astrophysics, Hadrons and quarks in nuclear matter, Quark matter

1. Introduction

Neutron star (NS) is a cosmic laboratory which provides us with a testing ground for the rich phase structure of quantum chromodynamics (QCD) [1] through the observables such as the mass (M), the radius (R), the surface temperature (T_s), the surface magnetic field (B_s) and so on [2]. Among others, M and R are particularly important probes for constraining the equation of state (EOS) and the composition of high density matter.

From the theoretical point of view, the onset of the strangeness degrees of freedom inside the NSs has attracted much attention in recent years: General consensus is that the hyperons (Y) such as Λ and Σ^- would participate in NS cores at densities of several times nuclear matter density ($\rho_0 = 0.17 \text{ fm}^{-3}$)[3–9]. The precise value of the threshold density ρ_{th} depends on the hyperon-nucleon interactions which have still uncertainties at the moment but will be improved by the future hypernuclear data [10–12] and by the lattice QCD simulations [13]. From the observational point of view, a massive NS, PSR J1614-2230, with $M_{\text{obs}} = (1.97 \pm 0.04)M_{\odot}$ was recently discovered [14]. Conflict between the $2M_{\odot}$ -NS which requires stiff EOS and the Y -mixing which gives soft EOS leads to a challenging problem whether massive neutron stars are in contradiction to the existence of the exotic components such as the hyperons and deconfined quarks[15–23].

[†]These authors contributed equally to this work.

The purpose of the present paper is to investigate whether the “hybrid stars” which have quark matter in the core are compatible with $2M_{\odot}$ -NS. Historically, the transition from the hadronic matter to the quark matter has been assumed to be the first-order phase transition and the Gibbs phase equilibrium conditions are imposed. However, treating the point-like hadron as an independent degree of freedom is not fully justified in the transition region because all hadrons are extended objects composed of quarks and gluons. Furthermore, the system must be strongly interacting in the transition region, so that it cannot be described neither by an extrapolation of the hadronic EOS from the low-density side nor by an extrapolation of the quark EOS from the high-density side [24]. This is analogous to the BEC-BCS crossover realized in the many-body system of ultra-cold fermionic atoms [25].

Fig. 1 illustrates the above situation in terms of the pressure as a function of baryon density (ρ). One may expect a gradual onset of quark degrees of freedom in dense matter associated with the percolation of finite size hadrons, i.e., a smooth crossover from the hadronic matter to the quark matter. Such a percolation picture of hadrons has been discussed in seminal works such as Refs.[26, 27]. Also, hadron-quark continuity [28, 29] and hadron-quark crossover [30, 31] have been discussed in relation to the existence of color superconductivity at high density. As we will show in this paper, the crossover picture does not necessarily lead to the softening of EOS unlike the case of first-order transition, so that it provides us with a novel mechanism to support massive neutron stars with quark core. Preliminary account of our results has been reported in [32].

This paper is organized as follows. In §2, the characteristic features of the hadronic EOSs (H-EOSs) to be used at low densities are summarized. In §3, we treat the strongly interacting quark matter by using the Nambu-Jona-Lasinio (NJL) type model and derive the quark EOS (Q-EOS) to be used at high densities. In §4, we describe our interpolation procedure

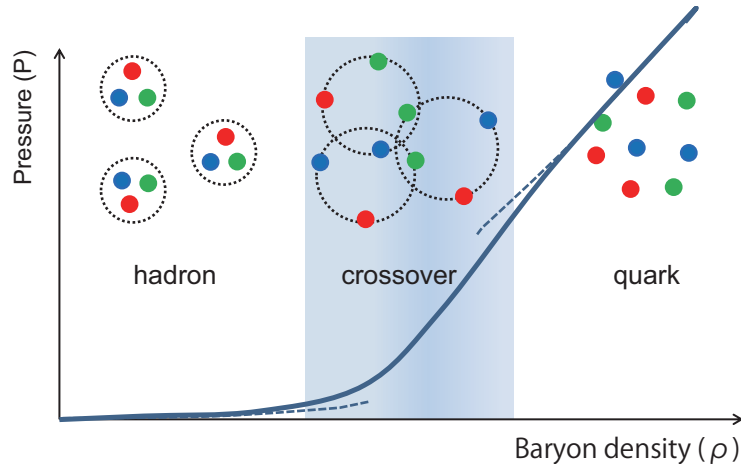


Fig. 1 Schematic picture of the QCD pressure (P) as a function of the baryon density (ρ) under the assumption of the hadron-quark crossover. The crossover region where finite-size hadrons start to overlap and percolate is shown by the shaded area. The pressure calculated on the basis of the point-like hadrons (shown by the dashed line at low density) and that calculated on the basis of weakly interacting quarks (shown by the dashed line at high density) lose their validity in the crossover region, so that the naive use of the Gibbs conditions by extrapolating the dashed lines is not justified in general.

to obtain the EOS in the hadron-quark crossover region. In §5, numerical results and discussions are given for the bulk properties of hybrid stars, such as the $M - R$ relationship, the maximum mass M_{\max} and the $M - \rho_c$ (central density) relationship. We discuss how these results depend on the different choice of H-EOS and Q-EOS. A comment on the cooling of NSs with respect to the hyperon mixture inside the core is also given. §6 is devoted to concluding remarks.

2. Hadronic EOS (H-EOS)

We consider several different EOSs with Y -mixing:

- TNI2, TNI3, TNI2u and TNI3u [33, 34]: TNI2 and TNI3 are obtained by the G-matrix calculation with Reid soft-core potential for NN and Nijmegen type-D hard-core potential for YN and YY . Also, a phenomenological three-body force [35] is introduced in a form of effective NN force to reproduce the saturation point of symmetric nuclear matter with the incompressibility $\kappa=250\text{MeV}$ (TNI2) and $\kappa=300\text{MeV}$ (TNI3). For TNI2u and TNI3u, the three-body interaction is introduced *universally* in a form of effective NN , NY and YY forces.
- AV18+TBF and Paris+TBF [36]: They are obtained by the G-matrix calculation but with different choice of potentials, AV18 and Paris potentials for NN and Nijmegen soft-core potential for YN and YY . Also, the three-body force of Urbana-type is introduced in a form of effective NN force to meet the saturation condition.
- SCL3 $\Lambda\Sigma$ [39]: It is based on a relativistic mean field (RMF) model with chiral SU(3) symmetry and logarithmic potential motivated by the strong coupling lattice QCD approach. Phenomenological parameters of the model are determined to reproduce the saturation condition, bulk properties of normal nuclei and separation energies of single- and double- Λ hypernuclei.

In Fig.2, we plot the pressure P for the Y -mixed neutron star matter with β -equilibrium and charge neutrality as a function of baryon density ρ obtained from the EOSs listed above (Paris+TBF is not shown since it is almost the same as AV18+TBF). For comparison, P for the neutron star matter without hyperons obtained from APR EOS ([40]) is also plotted in Fig.2 by the dotted lines. In Fig. 3, the $M - \rho_c$ relationships for corresponding NS models are shown. The filled circle on each curve denotes the threshold density of Y -mixture. There are some features to be remarked from the figure: (i) Different H-EOSs do not show significant difference in P up to $2.5 \rho_0$, and (ii) the Y -mixture is delayed from $(2-3)\rho_0$ to $4\rho_0$ if there exists repulsive three-body force universally for baryons as in the case of TNI2u and TNI3u. Even light-mass NSs ($M < M_\odot$ for TNI2, TNI3 and AV18+TBF and $M < 1.2M_\odot$ for SCL3 $\Lambda\Sigma$) have already the Y -mixed core.

In Table 1, we show κ and the threshold densities of hyperon-mixing, $\rho_{\text{th}}(\Lambda)$ and $\rho_{\text{th}}(\Sigma^-)$, for each H-EOS. In the same table, we show the maximum-mass M_{\max} , the radius R and the central density ρ_c of the NS obtained from each H-EOS. The values obtained by switching off the Y -mixing are given in the parentheses for comparison. For the H-EOSs without universal three-body repulsion, significant softening due to Y -mixing reduces M_{\max} , i.e., $M_{\max}(\text{without } Y)=(1.62 - 2.00) \rightarrow M_{\max}(\text{with } Y)=(1.08 - 1.26)$. This clearly contradicts the observed mass $M_{\text{obs}} = 1.44M_\odot$ for PSR1913+16. On the other hand, H-EOSs with universal three-body repulsion (TNI2u, TNI3u), M_{\max} is recovered nearly to that without Y .

Table 1 Properties of various hadronic EOSs with hyperons; TNI2, TNI3, TNI2u, TNI3u [33, 34], Paris+TBF, AV18+TBF [36–38] and SCL3 $\Lambda\Sigma$ [39]. κ is the nuclear incompressibility and ρ_{th} is the threshold density of hyperon-mixing with ρ_0 ($=0.17/\text{fm}^3$) being the normal nuclear density. R and ρ_c denote the radius and central density for the maximum mass (M_{max}) NS, respectively. The numbers in the parentheses are those without hyperons. *s indicate that the numbers are read from the figures in [36].

EOS	TNI2	TNI3	TNI2u	TNI3u	Paris+TBF	AV18+TBF	SCL3 $\Lambda\Sigma$
κ (MeV)	250	300	250	300	281	192	211
$\rho_{\text{th}}(\Lambda)/\rho_0$	2.95	2.45	4.01	4.01	2.9*	2.8*	2.24
$\rho_{\text{th}}(\Sigma^-)/\rho_0$	2.83	2.23	4.06	4.01	1.9*	1.8*	2.24
M_{max}/M_\odot	1.08 (1.62)	1.10 (1.88)	1.52	1.83	1.26 (2.06)	1.22 (2.00)	1.36 (1.65)
$R(\text{km})$	7.70 (8.64)	8.28 (9.46)	8.43	9.55	10.46 (10.50)	10.46 (10.54)	11.42 (10.79)
ρ_c/ρ_0	16.10 (9.97)	13.90 (8.29)	11.06	8.26	7.35 (6.47)	7.35 (6.53)	6.09 (6.85)

The use of several kinds of EOS mentioned above, from different theoretical methods (G-matrix, RMF), with various stiffness ranging from $\kappa \sim 190$ MeV to 300 MeV and with the variation of $\rho_{\text{th}}(Y) \simeq (2 - 4)\rho_0$, is expected to cover the present uncertainties of the H-EOSs.

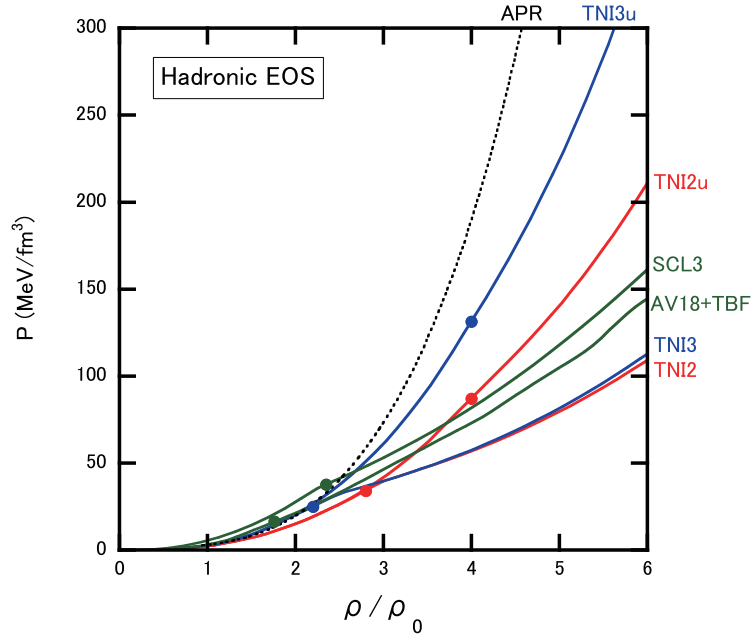


Fig. 2 Pressure (P) for the Y -mixed neutron star matter with β -equilibrium and charge neutrality as a function of the total baryon density ρ for different types of EOS. Solid red lines: TNI2u (G-matrix approach, universal three-body force, $\kappa = 250\text{MeV}$) and TNI2 (G-matrix approach, three-nucleon force, $\kappa = 250\text{MeV}$). Solid blue lines: TNI3u (G-matrix approach, universal three-body force, $\kappa = 300\text{MeV}$) and TNI3 (G-matrix approach, three-nucleon force, $\kappa = 300\text{MeV}$) [33, 34]. Solid green lines: AV18+TBF (G-matrix approach, three-nucleon force, $\kappa = 192\text{MeV}$) [36] and SCL3 $\Lambda\Sigma$ (relativistic mean field model with chiral SU(3) symmetry, $\kappa = 211\text{MeV}$) [39]. Paris+TBF is not plotted here because it is almost the same as AV18+TBF. For comparison, P for the neutron star matter without hyperons obtained from APR EOS [40] is also plotted by the dotted lines.

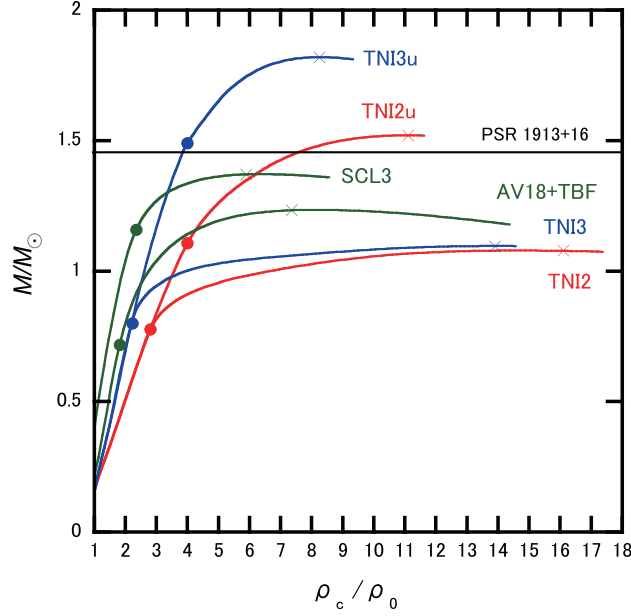


Fig. 3 M - ρ_c relationship corresponding to EOSs in Fig.2 (details of EOS are given in Table A1 of Appendix A). Colors on each line are the same with those in Fig.2. The cross symbols denote the points where the NS mass becomes maximum, M_{max} . Solid black line denotes $M = 1.44M_{\odot}$ for PSR 1913+16.

For completeness, numerical values of the pressure P and the energy density ε as a function of the baryon density are tabulated in Table A1 in Appendix A.

3. Quark EOS (Q-EOS)

The baryon density at the central core of the NSs would be at most $10\rho_0$. Although hadrons do not keep their identities in such a high density, the chemical potential of the quarks are about $(400 - 500)\text{MeV}$ which is not high enough for the asymptotic freedom at work. Namely, the deconfined quarks inside the NSs, even if they exist, would be strongly interacting. Analogous situation at finite temperature has been expected theoretically and is recently confirmed by the relativistic heavy-ion collisions at RHIC and LHC; it is now called the strongly interacting quark-gluon plasma (sQGP).

Since lattice QCD to treat the strongly interacting quark matter (sQM) at finite baryon density is unfortunately not possible due to the notorious sign problem, we adopt an effective theory of QCD, the $(2+1)$ -flavor Nambu–Jona-Lasinio (NJL) model. This model is particularly useful to take into account the important phenomena such as the partial restoration of chiral symmetry at high density [41–44].

The model Lagrangian we consider is

$$\begin{aligned} \mathcal{L}_{\text{NJL}} = & \bar{q}(i\cancel{\partial} - m)q + \frac{1}{2}G_s \sum_{a=0}^8 [(\bar{q}\lambda^a q)^2 + (\bar{q}i\gamma_5\lambda^a q)^2] - G_b [\det \bar{q}(1 + \gamma_5)q + \text{h.c.}] \\ & - \left\{ \frac{1}{2}g_v (\bar{q}\gamma^\mu q)^2 \right. \\ & \left. - \frac{1}{2}G_v \sum_{a=0}^8 [(\bar{q}\gamma^\mu\lambda^a q)^2 + (\bar{q}i\gamma^\mu\gamma_5\lambda^a q)^2] \right\} \end{aligned} \quad (1)$$

where the quark field q_i ($i = u, d, s$) has three colors and three flavors with the current quark mass m_i . The term proportional to G_s is a $U(3)_L \times U(3)_R$ symmetric four-fermi interaction where λ^a are the Gell-Mann matrices with $\lambda^0 = \sqrt{2/3} \mathbf{I}$. The term proportional to G_D is the Kobayashi–Maskawa–’t Hooft (KMT) six-fermi interaction which breaks $U(1)_A$ symmetry. We consider two types of vector interaction (the second line of Eq.(1)): The term proportional to $g_v (> 0)$ gives a universal repulsion among different flavors, while the one proportional to $G_v (> 0)$ gives flavor-dependent repulsion.

In the mean-field approximation, the constituent quark masses M_i ($i = u, d, s$) are generated dynamically through the NJL interactions ($G_{S,D}$),

$$M_i = m_i - 2G_s \sigma_i + 2G_D \sigma_j \sigma_k, \quad (2)$$

where $\sigma_i = \langle \bar{q}_i q_i \rangle$ is the quark condensate in each flavor, and (i, j, k) corresponds to the cyclic permutation of u, d and s . The thermodynamic potential Ω is related to the pressure as $\Omega = -T \log Z = -PV$, so that we have

$$\begin{aligned} P(T, \mu_{u,d,s}) = & T \sum_i \sum_\ell \int \frac{d^3 p}{(2\pi)^3} \text{Tr} \ln \left(\frac{S_i^{-1}(i\omega_\ell, \mathbf{p})}{T} \right) \\ & - G_s \sum_i \sigma_i^2 - 4G_D \sigma_u \sigma_d \sigma_s + \left\{ \frac{1}{2} g_v (\sum_i n_i)^2 \right. \\ & \left. + \frac{1}{2} G_v \sum_i n_i^2 \right\} \end{aligned} \quad (3)$$

where $n_i = \langle q_i^\dagger q_i \rangle$ is the quark number density in each flavor, and S_i is the quark propagator, which can be written as

$$S_i^{-1} = \not{p} - M_i - \gamma^0 \mu_i^{\text{eff}}, \quad \mu_i^{\text{eff}} \equiv \begin{cases} \mu_i - g_v \sum_j n_j \\ \mu_i - G_v n_i \end{cases} \quad (4)$$

where $i\omega_\ell = (2\ell + 1)\pi T$ and μ_i^{eff} is an effective chemical potential [45].

There are six independent parameters in the (2+1)-flavor NJL model; the UV cutoff, Λ , the coupling constants, G_s, G_D and $g_v (G_v)$, and the quark masses, $m_{u,d}$ and m_s . Five parameters except for $g_v (G_v)$ have been determined from hadron phenomenology. We consider three parameter sets summarized in Table 2; HK (Hatsuda and Kunihiro), RKH (Rehberg, Klevansky and Hufner) and LKW (Lutz, Klimt and Weise) [41–44].

Table 2 Parameter sets of (2+1)-flavor NJL model [41–44].

	$\Lambda(\text{MeV})$	$G_s \Lambda^2$	$G_D \Lambda^5$	$m_{u,d}(\text{MeV})$	$m_s(\text{MeV})$
HK	631.4	3.67	9.29	5.5	135.7
RKH	602.3	3.67	12.36	5.5	140.7
LKW	750	3.64	8.9	3.6	87

The magnitude of $g_v (G_v)$ has not been determined well: Recent studies of the PNJL model applied to the QCD phase diagram suggest that g_v may be comparable to or larger than G_s

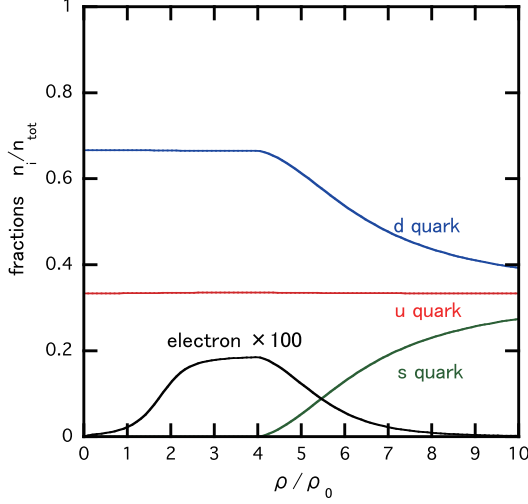


Fig. 4 The number fractions ($n_{u,d,s,e}/n_{\text{tot}}$ with $n_{\text{tot}} = n_u + n_d + n_s = 3\rho$) as a function of the baryon density ρ . Solid red line: The fraction of u quark. Solid blue line: The fraction of d quark. Solid green line: The fraction of s quark. Solid black line: The fraction of electron $\times 100$. Muon does not appear due to the emergence of s quarks.

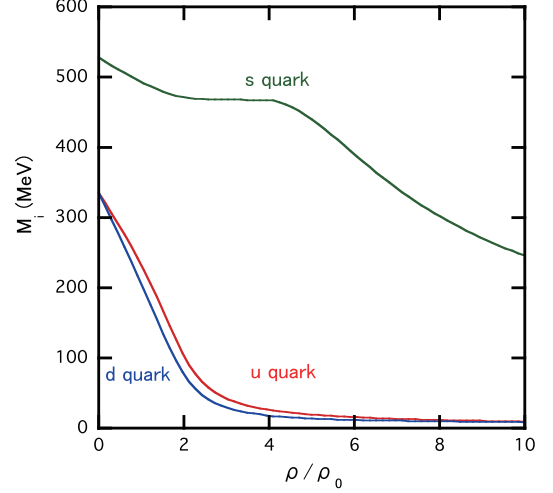


Fig. 5 The constituent quark masses (M_i) as a function of ρ . Colors on each line are the same with those in Fig.4.

[46, 47], so that we change its magnitude in the following range,

$$0 \leq \frac{g_v}{G_s} \leq 1.5. \quad (5)$$

In §4 and §5, we will show our results mainly for the HK parameter set with the vector interaction of the g_v type. Later, we discuss how the results change in other cases. The Q-EOS with strangeness is obtained from the above model under two conditions: (i) the charge neutrality among quarks and leptons, i.e. $\frac{2}{3}n_u - \frac{1}{3}n_d - \frac{1}{3}n_s - n_e - n_\mu = 0$, and (ii) the β -equilibrium among quarks and leptons, i.e. $\mu_d = \mu_s = \mu_u + \mu_e$ and $\mu_e = \mu_\mu$.

In Fig.4, the number fractions ($n_{u,d,s,e}/n_{\text{tot}}$ with $n_{\text{tot}} = n_u + n_d + n_s = 3\rho$) as a function of the baryon density ρ are plotted. Also, in Fig.5, the constituent quark masses (M_i) as a function of ρ are plotted. The HK parameter set with the g_v -type interaction are used in both figures. The flavor-independent g_v -type interaction leads to a pressure in Eq.(3) depending only on μ_i^{eff} . Then, the number fractions and the quark masses as a function of ρ do not depend on g_v .

At low baryon densities below a threshold density $\rho_{\text{th}} \simeq 4\rho_0$, the system is composed of only u, d and e with $n_d \sim 2n_u$ due to charge neutrality and β -equilibrium (Fig.4). In this region, the strong interaction among quarks (mainly the G_s -term in the NJL model) drives the partial restoration of chiral symmetry and hence a rapid decrease of the constituent masses $M_{u,d}$ (Fig.5). Due to the coupling between different flavors through the G_d -term, the strange quark mass M_s in the Dirac sea is also affected slightly.

When the baryon density exceeds ρ_{th} , the chemical potential of the strange quark μ_s becomes larger than the strange quark mass ($\mu_s > M_s$), so that the system starts to have the strangeness degree of freedom. Since the strange quark is negatively charged, the electrons start to disappear from the system and the d quark fraction gets decreased at the same time

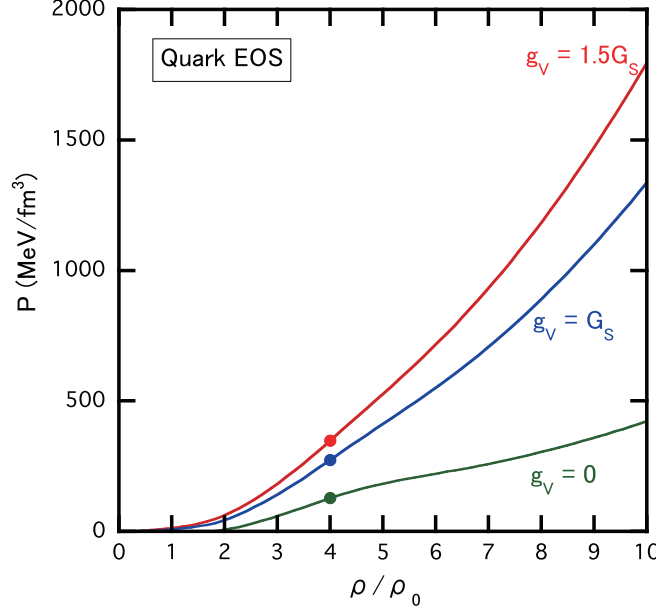


Fig. 6 Pressure (P) as a function of baryon density ρ in a pure quark matter for the HK parameter set with $g_v/G_s = 0, 1.0, 1.5$. The filled circles denote the onset of the strangeness.

(Fig.4). We note that the system does not have the muon, because the electron chemical potential is smaller than $m_\mu=106\text{MeV}$ at all densities. In the high density limit, system approaches to the flavor symmetric u, d, s matter without leptons. Once the s -quark appears in the system, M_s is also suppressed mainly due to the G_s -term (Fig.5). The strangeness threshold ρ_{th} does not depend on g_v as already mentioned, while it depends on the NJL parameter sets in Table 2; $\rho_{\text{th}}/\rho_0 = 4.0, 3.9$ and 3.0 for HK, RKH and LKW, respectively.

In Fig.6, we plot the pressure(P) of the strongly interacting quark matter for the HK parameter set with different values of the vector coupling ($g_v/G_s = 0, 1.0, 1.5$ according to Eq.(5)). Due to the universal repulsion of the g_v -type vector interaction, the Q-EOS becomes stiffer as g_v increases. As mentioned already, the onset density of the strangeness (marked by the filled circles) does not depend on g_v . We note here that the present Q-EOS has a first-order phase transition below $2\rho_0$ for $g_v < 0.3G_s$. However, it does not affect the final results of the present paper, since such a low density region is dominated by the hadronic EOS in our hadron-quark crossover approach to be discussed in §4.

4. Hadron-Quark crossover

As discussed in §1, treating the point-like hadron as an independent degree of freedom loses its validity as the baryon density approaches to the percolation region. In other words, the system cannot be described neither by an extrapolation of the hadronic EOS from the low-density side nor by an extrapolation of the quark EOS from the high-density side. Under such situation, it does not make much sense to apply the Gibbs criterion of two phases I and II, $P_I(T_c, \mu_c) = P_{II}(T_c, \mu_c)$ since P_I and P_{II} are not reliable in the transition region.

Since the first principle QCD calculation at high baryon density is not available and effective models at finite baryon density with proper treatment of the confinement phenomena do not

exist at present, we will consider a phenomenological “interpolation” between the H-EOS and Q-EOS as a first step. Such an interpolation is certainly not unique, but we adopt a simplest one²;

$$P(\rho) = P_H(\rho)f_-(\rho) + P_Q(\rho)f_+(\rho), \quad (6)$$

$$f_{\pm}(\rho) = \frac{1}{2} \left(1 \pm \tanh \left(\frac{\rho - \bar{\rho}}{\Gamma} \right) \right), \quad (7)$$

where P_H and P_Q are the pressure in the hadronic matter and that in the quark matter, respectively. The window $\bar{\rho} - \Gamma \lesssim \rho \lesssim \bar{\rho} + \Gamma$ characterizes the crossover region in which both hadrons and quarks are strongly interacting, so that neither pure hadronic EOS nor pure quark EOS are reliable. The percolation picture illustrated in Fig.1 is best implemented by the interpolation in terms of the baryon density ρ instead of the baryon chemical potential.

One should not confuse Eq.(7) with the pressure in the mixed phase associated with the first-order phase transition in which f_{\pm} is considered to the volume fraction of each phase. In our crossover picture, the system is always uniform and f_- (f_+) should be interpreted as the degree of reliability of H-EOS (Q-EOS) at given baryon density.

To calculate the energy density ε as a function of ρ in thermodynamically consistent way, we integrate the thermodynamical relation, $P = \rho^2 \partial(\varepsilon/\rho)/\partial\rho$ and obtain

$$\varepsilon(\rho) = \varepsilon_H(\rho)f_-(\rho) + \varepsilon_Q(\rho)f_+(\rho) + \Delta\varepsilon \quad (8)$$

$$\Delta\varepsilon = \rho \int_{\bar{\rho}}^{\rho} (\varepsilon_H(\rho') - \varepsilon_Q(\rho')) \frac{g(\rho')}{\rho'} d\rho' \quad (9)$$

with $g(\rho) = \frac{2}{\Gamma}(e^X + e^{-X})^{-2}$ and $X = (\rho - \bar{\rho})/\Gamma$. Here ε_H (ε_Q) is the energy density obtained from H-EOS (Q-EOS). $\Delta\varepsilon$ is an extra term which guarantees the thermodynamic consistency.

In the following, we consider crossover window which satisfies the following physical conditions: (i) The system is always thermodynamically stable $dP/d\rho > 0$, and (ii) the normal nuclear matter is well described by the H-EOS so that $\bar{\rho} - 2\Gamma > \rho_0$ is satisfied. Shown in Fig.7 is an example of the interpolation between TNI2u for H-EOS and NJL with $g_v = G_s$ for Q-EOS according to Eq.(7). The crossover window is chosen to be $(\bar{\rho}, \Gamma) = (3\rho_0, \rho_0)$ and is shown by the shaded area on the horizontal axis. An important lesson one can learn from Fig.7 is that the H-EOS (Q-EOS) is nothing more than the asymptotic form of the “true” $P(\rho)$ around $\rho = 0$ ($\rho = \infty$). Therefore, naive extrapolation of H-EOS and Q-EOS beyond their applicability would miss essential physics.

In Fig.8, we plot the interpolated EOS using TNI2u and NJL for different values of g_v in a wide range of baryon density. The filled circles denote the onset of strangeness degrees of freedom, either hyperons or strange quarks. In the next section, we will solve the structure of hybrid stars mainly by using these EOSs.

² Similar interpolating function f_{\pm} has been previously considered at finite temperature in [48].

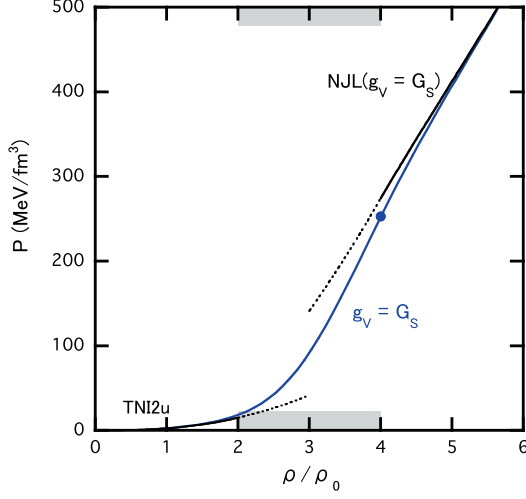


Fig. 7 The interpolated pressure between TNI2u H-EOS and NJL Q-EOS with $g_V = G_s$ for $(\bar{\rho}, \Gamma) = (3\rho_0, \rho_0)$. Pressure is illustrated by a blue line. The filled circle denotes the threshold density of strangeness.

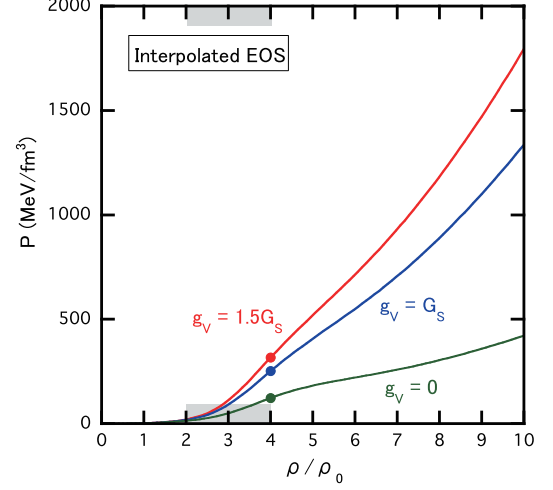


Fig. 8 Interpolated pressure (P) as a function of baryon density ρ for the case $(\bar{\rho}, \Gamma) = (3\rho_0, \rho_0)$ with $g_V/G_s = 0, 1.0, 1.5$.

5. Numerical results and discussions

5.1. Massive hybrid star with strangeness

We now solve the following Tolman-Oppenheimer-Volkov (TOV) equation to obtain M - R relationship by using the EOSs with and without the hadron-quark crossover:

$$\begin{aligned} \frac{dP}{dr} &= -\frac{G}{r^2} (M(r) + 4\pi P r^3) (\varepsilon + P) (1 - 2GM(r)/r)^{-1}, \\ M(r) &= \int_0^r 4\pi r'^2 \varepsilon(r') dr', \end{aligned} \quad (10)$$

where we have assumed the spherical symmetry with r being the radial distance from the center of the star.

In Fig. 9(a), we show the M - R relationship for various H-EOSs with hyperons whose onset is denoted by the filled circles. The crosses denote the points where maximum masses are realized: In all cases, M_{\max} does not reach $2M_\odot$ due to the softening of EOS by the hyperon mixture.

In Fig. 9(b), we show the M - R relationship with the EOS interpolated between H-EOS and Q-EOS: For the H-EOS, we consider the same EOSs as shown in Fig. 9(a), while for the Q-EOS, we adopt the HK-parameter set with $g_V = G_s$ as a typical example. The crossover window is fixed to be $(\bar{\rho}, \Gamma) = (3\rho_0, \rho_0)$. Cases for different parameters in Q-EOS as well as for different window parameters are discussed in the next subsection.

The red lines in Fig. 9(b) correspond to the cases with TNI2u and TNI2, the blue lines correspond to TNI3u and TNI3, and the green lines correspond to SCL3A Σ and AV18+TBF. The onset of strangeness and the maximum mass are denoted by the filled circles and the crosses, respectively. Irrespective of the H-EOSs, the interpolated EOS can sustain hybrid star with $M_{\max} > 2M_\odot$: A smooth crossover around $\rho \sim 3\rho_0$ and the stiff Q-EOS due to repulsive vector interaction are two fundamental reasons behind this fact. Also, we note that the radius of the hybrid star with interpolated EOS is in a range $R = (11 \pm 1)\text{km}$ for

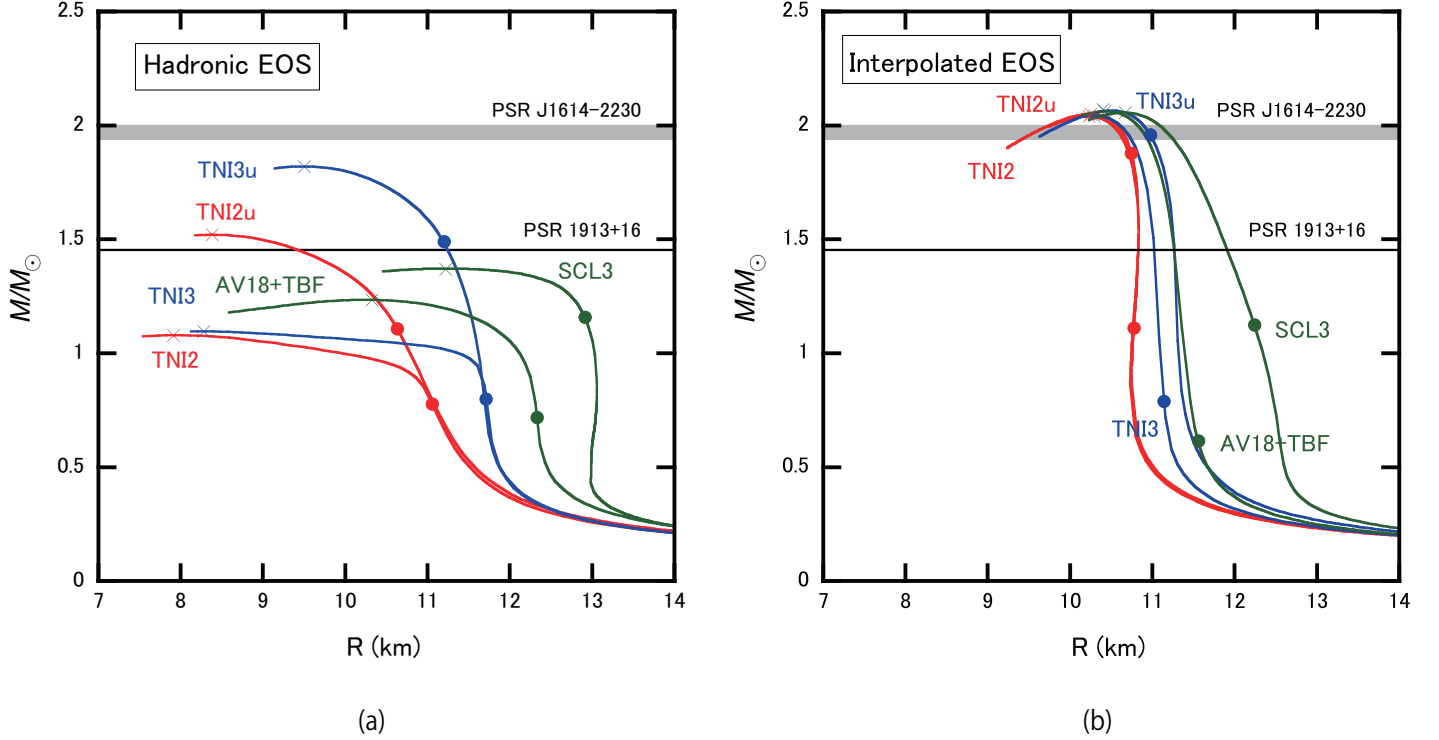


Fig. 9 $M-R$ relationships. (a) $M-R$ relationships with various H-EOS including hyperons. Solid red lines: TNI2u (universal 3-body force with $\kappa = 250\text{MeV}$) and TNI2 (3-nucleon force with $\kappa = 250\text{MeV}$). Solid blue lines: TNI3u (universal 3-body force with $\kappa = 300\text{MeV}$) and TNI3 (3-nucleon force with $\kappa = 300\text{MeV}$) [33, 34]. Solid green lines: AV18+TBF (G-matrix approach with hyperons) [36] and SCL3 $\Lambda\Sigma$ (Relativistic mean field model with a chiral SU(3) symmetry) [39]. The gray band denotes $M = (1.97 \pm 0.04)M_\odot$ for PSR J1614-2230. The solid black line denotes $M = 1.44M_\odot$ for PSR 1913+16. (b) $M-R$ relationship with the EOS interpolated between H-EOS in (a) and Q-EOS with the HK parameter set and $g_V = G_S$, by the window parameters $(\bar{\rho}, \Gamma) = (3\rho_0, \rho_0)$. Colors on each line are the same with those in (a).

$0.5 < M/M_\odot < 2.0$, except for the case of SCL3 $\Lambda\Sigma$.² Such a narrow window of R independent of the values of M is consistent with the phenomenological constraints on R based on recent observations of both transiently accreting and bursting sources [49, 50].

In Table 3, we show the maximum mass and the associated central density of the hybrid star with the interpolated EOS with $g_V = G_S$ and $g_V = 1.5G_S$. In all combinations of H-EOS and Q-EOS, M_{max} exceeds $2M_\odot$ with the central density, $\rho_c = (5.4 - 6.1)\rho_0$.

Let us now turn to the internal structure of the hybrid star, in particular its strangeness content. From the location of the filled circles in Fig. 9(b), one finds that the flavor-independent universal three-baryon repulsion in TNI2u and TNI3u increases the onset density of the strangeness inside the hybrid star. This can be seen more explicitly by plotting the radial profile of the hybrid star: The upper panels of Fig. 10 show the $\rho-r$ relationships for $2M_\odot$ and $1.44M_\odot$ hybrid stars with TNI2 (left) and TNI2u (right). The threshold densities of the strangeness given in Table 1 are indicated by the double lines. In our interpolated EOSs, the

² The reason why the case with SCL3 $\Lambda\Sigma$ is different from others can be easily seen from Fig. 2: The pressure P of SCL3 $\Lambda\Sigma$ is nearly twice as large as that of the other EOSs at $\rho = (1 - 2)\rho_0$. This leads to a larger R of light NSs.

Table 3 M_{max}/M_{\odot} (ρ_c/ρ_0) for different choice of H-EOS and difference stiffness of Q-EOS.

H-EOS	$g_v = G_s$	$g_v = 1.5G_s$
TNI2u	2.05 (6.1)	2.17 (5.5)
TNI2	2.04 (6.1)	2.16 (5.9)
TNI3u	2.07 (5.9)	2.18 (5.4)
TNI3	2.04 (6.1)	2.16 (5.5)
Paris+TBF	2.06 (6.1)	2.17 (5.6)
AV18+TBF	2.06 (6.1)	2.17 (5.5)
SCL3 $\Lambda\Sigma$	2.06 (5.9)	2.17 (5.5)

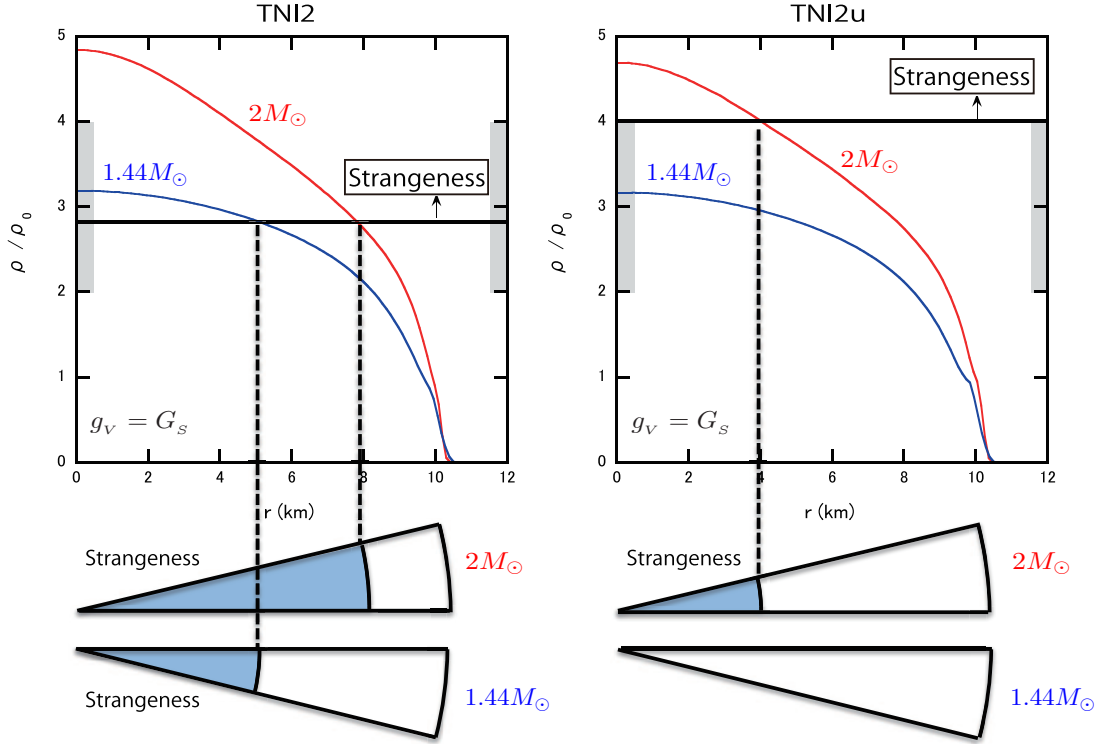


Fig. 10 Density-profiles $\rho(r)$ with r being the distance from the center for the $2.0M_{\odot}$ star (red line) and $1.44M_{\odot}$ star (blue line). In the left upper panel TNI2 H-EOS and Q-EOS with $g_v = G_s$ and the HK parameter set are used in the interpolation with the window parameters $(\bar{\rho}, \Gamma) = (3\rho_0, \rho_0)$, while in the right upper panel TNI2u H-EOS and Q-EOS above are used. Double line shows the density above which the strangeness appears. Lower illustrations show the internal structure. Only the shaded regions contain strangeness degrees of freedom.

above stars turn out to have almost the same radius. The lower illustrations of Fig.10 show the cross sections of the corresponding hybrid stars.

These figures imply that, even if the mass and the radius are the same, the strangeness content of the hybrid stars can be quite different. This point is of particular interest for the cooling problem of NSs. As is well known, NSs with a Y -mixed core undergo an extremely rapid cooling due to the efficient ν -emission processes called “hyperon direct URCA” (Y -Durca, e.g., $\Lambda \rightarrow p + e^- + \bar{\nu}_e$, $p + e^- \rightarrow \Lambda + \nu_e$) and are cooled very rapidly below the

detection limit of thermal X-ray. Therefore, for the NSs consisting of pure hadronic components with Y , only the very light-mass NSs ($M < (1.0 - 1.2)M_\odot$, as in Fig. 3) can escape from Y -Durca rapid cooling. This means an unlikely situation that all the NSs whose T_s are observed should be light-mass stars in spite of the fact that the observed mass distribution is centered around $(1.4 - 1.5)M_\odot$ [2]. On the contrary, in the case of the hybrid star with $g_v = G_s(1.5G_s)$ under consideration, NSs as heavy as up to $1.9(2.0)M_\odot$ can avoid this rapid cooling, allowing the T_s -observed NSs to be from the light-mass to heavy mass stars ($M \leq (1.9 - 2.0)M_\odot$, as in Fig. 11).

It is in order here to comment on the relationship between the maximum mass and the nuclear incompressibility κ . From the properties of finite nuclei, the nuclear incompressibility κ is estimated to be $(240 \pm 20)\text{MeV}$ [51]. The interpolated EOSs with TNI2 and TNI2u are consistent with this empirical κ , and yet they can reach $M_{\text{max}} > 2M_\odot$. In other words, what is important to sustain massive hybrid stars is not the value of the incompressibility, but the stiffness of the EOS at and above $\sim 3\rho_0$.

5.2. Dependence on Q-EOS

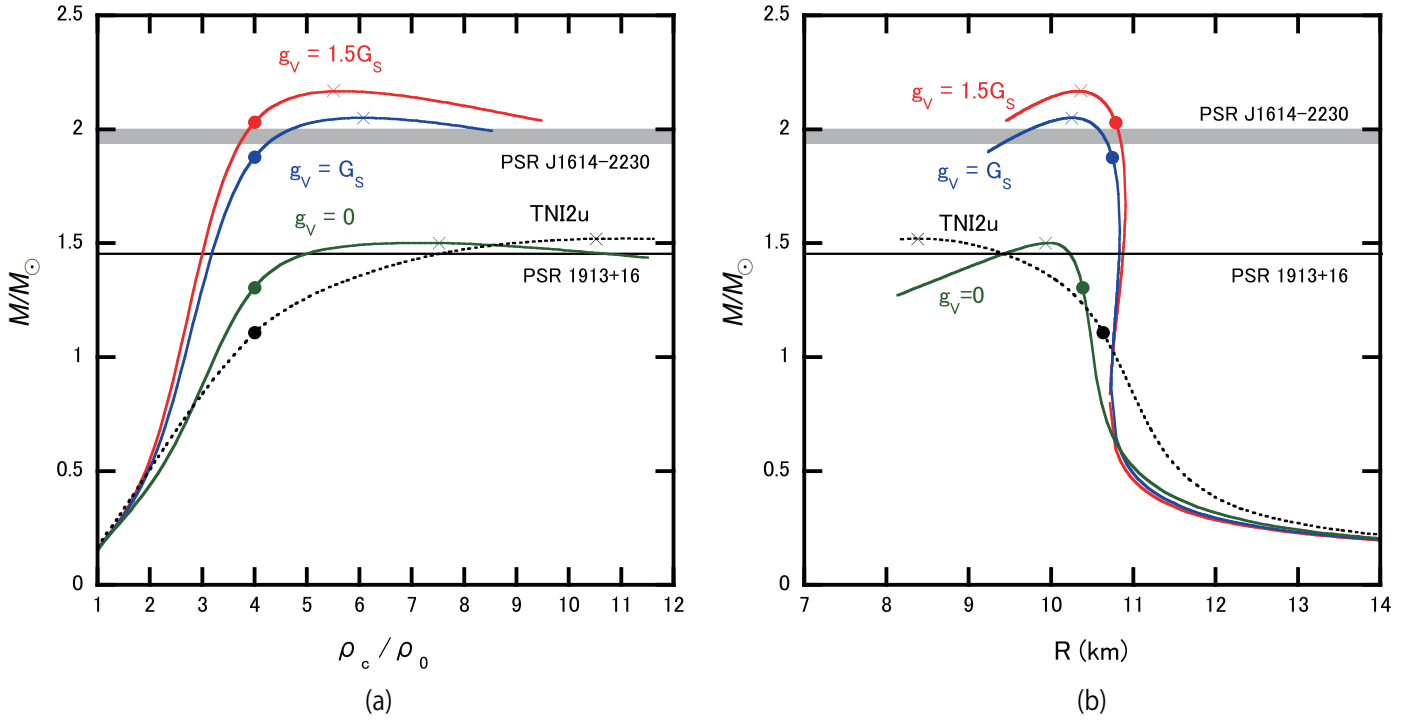


Fig. 11 (a) $M - \rho_c$ relationships with the interpolated EOSs. We adopt the HK-parameter set for the Q-EOS with various $g_v/G_s = 0, 1.0, 1.5$. The crossover window are fixed to be $(\bar{\rho}, \Gamma) = (3\rho_0, \rho_0)$. The cross symbols denote the points of M_{max} , while the filled circles denote the points beyond which the strangeness appears. The gray band denotes $M = (1.97 \pm 0.04)M_\odot$ for PSR J1614-2230. The solid black line denotes $M = 1.44M_\odot$ for PSR 1913+16. (b) $M - R$ relationships with the interpolated EOSs.

To see how the hybrid star structure changes by the stiffness of Q-EOS, we plot $M - \rho_c$ relationship for $g_v/G_s = 0, 1.0, 1.5$ with HK parameter set in Fig.11(a). We take TNI2u for

H-EOS and the same crossover window as in Fig.9. For comparison, the $M - \rho_c$ relationship only with TNI2u is plotted by the dashed line. Fig.11(b) shows the corresponding $M - R$ relations. As anticipated, M_{\max} increases as g_v increases. In Table 4, we show how M_{\max} and ρ_c depend on the choice of g_v and the choice of the NJL parameter set. Although the parameter dependence is not entirely negligible, the massive hybrid star is possible for sufficiently large values of g_v .

Table 4 The values of M_{\max}/M_{\odot} (ρ_c/ρ_0) for $g_v/G_S = 1.0, 1.5, 2.0$ with $(\bar{\rho}, \Gamma) = (3\rho_0, \rho_0)$ and TNI2u. The parameter sets of the NJL model, HK, RKH and LKW, are given in Table 2.

Q-EOS	$g_v=G_S$	$g_v=1.5G_S$	$g_v=2G_S$
HK	2.05 (6.1)	2.17 (5.5)	2.24 (5.4)
RKH	1.99 (6.2)	2.12 (5.8)	2.20 (5.4)
LKW	1.72 (7.5)	1.87 (6.7)	1.97 (6.3)

Finally, we consider the flavor-dependent vector interaction proportional to G_v given in Eq.(1). In the high density limit where u, d, s quarks have equal population, $\langle u^\dagger u \rangle = \langle d^\dagger d \rangle = \langle s^\dagger s \rangle$, the g_v interaction and the G_v interaction have the same contribution to the pressure in the mean-field approximation if we make the identification, $G_v = \frac{3}{2}g_v$. Motivated by this relation, we show M_{\max} and ρ_c for $G_v/G_S = 1.5, 2.25, 3.0$ in Table 5. For the density relevant to the core of the hybrid stars, the flavor SU(3) limit is not yet achieved due to the s -quark mass (see Fig. 4). Therefore, the EOS for the flavor-dependent repulsion with $G_v = \frac{3}{2}g_v$ is softer than the flavor independent repulsion with g_v . This can be seen by comparing the corresponding values in Table 5 and those in Table 4. In any case, the massive hybrid star is possible for sufficiently large values of G_v .

Table 5 M_{\max}/M_{\odot} (ρ_c/ρ_0) for the HK parameter set with the flavor-dependent repulsion G_S . The crossover window is $(\bar{\rho}, \Gamma) = (3\rho_0, \rho_0)$ and the hadronic EOS is TNI2u.

$G_v=1.5G_S$	$G_v=2.25G_S$	$G_v=3.0G_S$
1.87 (6.6)	1.99 (6.2)	2.07 (5.8)

5.3. Dependence on crossover window

In Table 6, we show M_{\max} and ρ_c for different choice of the crossover window parameterized by $\bar{\rho}$ and Γ . TNI2u and HK parameter set are adopted for H-EOS and Q-EOS, respectively. As the crossover window becomes lower and/or wider in baryon density, the interpolated EOS becomes stiffer and M_{\max} becomes larger. To be compatible with the observed massive NS with $M = (1.97 \pm 0.04)M_{\odot}$, the crossover needs to occur in $(2 - 4)\rho_0$.

5.4. Sound velocity of interpolated EOS

One of the measures to quantify the stiffness of EOS is the sound velocity $v_s = \sqrt{dP/d\varepsilon}$. In Fig.12, we plot v_s for our interpolated EOS with $g_v/G_S = 0, 1.0, 1.5$ as a function of ρ . The

Table 6 M_{\max}/M_{\odot} (ρ_c/ρ_0) under the variation of the parameters, $\bar{\rho}$ and Γ , which characterize the crossover window. H-EOS and Q-EOS are obtained from TNI2u and HK parameter set, respectively. Columns without numbers are the excluded cases corresponding to $\bar{\rho} - 2\Gamma < \rho_0$ in §4.

$\bar{\rho}$	$\Gamma/\rho_0 = 1$		$\Gamma/\rho_0 = 2$	
	$g_v = G_S$	$g_v = 1.5G_S$	$g_v = G_S$	$g_v = 1.5G_S$
$3\rho_0$	2.05 (6.1)	2.17 (5.5)	—	—
$4\rho_0$	1.89 (7.2)	1.97 (6.8)	—	—
$5\rho_0$	1.73 (8.2)	1.79 (8.0)	1.74 (8.0)	1.80 (7.7)
$6\rho_0$	1.60 (9.6)	1.64 (9.3)	1.62 (9.2)	1.66 (9.0)

kinks of v_s at $\rho \simeq 4\rho_0$ are caused by the softening of EOS by the appearance of strangeness. The enhancement of v_s of the interpolated EOS relative to the pure hadronic EOS takes place just at and above the crossover window.

5.5. Stability of hybrid star

The neutron star is gravitationally stable if the average adiabatic index $\bar{\Gamma}$ satisfies the inequality [52]:

$$\bar{\Gamma} = \frac{\int_0^R \Gamma P d^3r}{\int_0^R P d^3r} > \frac{4}{3} + \lambda \frac{GM}{R}. \quad (11)$$

Here $\Gamma = d \ln P / d \ln \varepsilon$ is the adiabatic index. Also, $\lambda GM/R$ with λ being a numerical constant of order unity is a general relativistic correction whose magnitude is much less than 1. Since

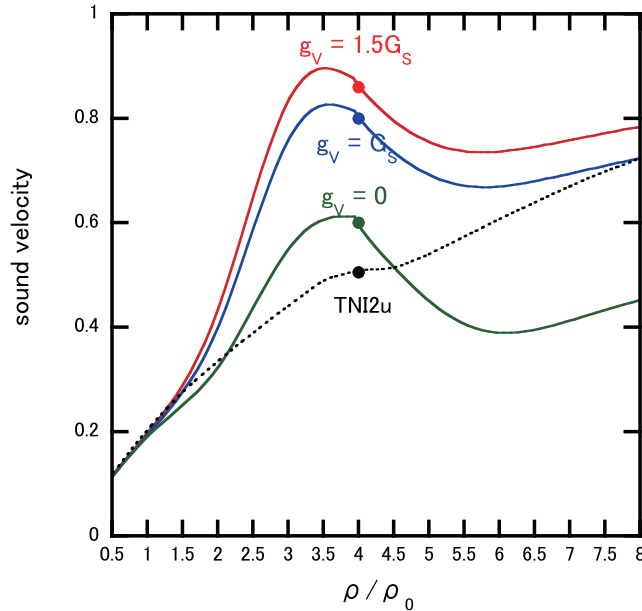


Fig. 12 Sound velocity v_s as a function of baryon density ρ . Solid lines: $v_s - \rho$ obtained from the interpolated EOS between the H-EOS with TNI2u and the Q-EOS with $g_v/G_S = 0, 1.0, 1.5$. The crossover window is $(2 - 4)\rho_0$. Dotted line : that for pure H-EOS with TNI2u. The filled circles denote the points beyond which strangeness starts to appear.

Γ of our H-EOS is about 2 at all densities and Γ of our Q-EOS is larger than $4/3$ due to the constituent quark mass and the repulsive vector interaction, Eq.(11) is always satisfied and our hybrid star is gravitationally stable.

6. Summary and concluding remarks

Recent observation of a two-solar mass NS presents a challenging problem how to reconcile stiff EOS suggested from the observational side with soft EOS due to hyperon-mixing from the theoretical side. In this paper we have studied this problem on the basis of the percolation picture from the hadronic matter with hyperons to the quark matter with strange quarks. We have constructed an EOS by the interpolation between the H-EOS at lower densities and the Q-EOS at higher densities, and found that the hybrid stars could have $M_{\max} \sim 2M_{\odot}$, compatible with the observation. This conclusion is in contrast to the conventional EOS for hybrid stars derived through the Gibbs construction in which the resultant EOS becomes always softer than hadronic EOS and thereby leads to smaller M_{\max} .

Our qualitative conclusion is insensitive to the choice of different types of H-EOS and different types of vector interaction in Q-EOS, as far as (i) the crossover between the hadronic matter and the quark matter proceeds in a relatively low density region, e.g., $\rho = (2 - 4)\rho_0$, and (ii) the quark matter is strongly interacting ($g_v/G_s \sim (1 - 2)$). We found that the sound velocity v_s , which increases rapidly in the crossover window for $g_v/G_s \geq 1$, can nicely characterize the stiffening of the interpolated EOS and associated enhancement of M_{\max} . By increasing g_v further, we can have hybrid stars close to the causality limit, $M_{\max} \sim 2.4M_{\odot}$.

The idea of rapid stiffening of the EOS starting from $2\rho_0$ opens a possibility that the experimental nuclear incompressibility $\kappa = (240 \pm 20)\text{MeV}$ at $\rho \sim \rho_0$ is compatible with the existence of massive neutron stars. Also, the idea may well be checked by independent laboratory experiments with medium-energy heavy-ion collisions.

Although the M - R relationship and M_{\max} are insensitive to the existence of the universal three-body repulsion, the onset density of strangeness is rather sensitive to such repulsion. If we have three-body repulsion acting universally among baryons, most of the hybrid stars with $M \leq (1.9 - 2.0)M_{\odot}$ are free from the extremely efficient hyperon direct-Urca cooling process and can avoid contradiction to observations.

Finally, we remark that the crossover region may contain richer non-perturbative phases such as color superconductivity, inhomogeneous structures and so on [1]. How these structures as well as the associated cooling processes affect the results of the present paper would be an interesting future problem to be examined.

Acknowledgment

K.M. and T.H. thank Wolfram Weise for discussions. T.T. thanks Ryoza Tamagaki, Toshitaka Tatsumi and Shigeru Nishizaki for discussions and interests in this work. We also thank K. Tsubakihara and A. Ohnishi for providing us with the numerical data of the SCL3 EOS. This research was supported in part by MEXT Grant-in-Aid for Scientific Research on Innovative Areas(No.2004:20105003) by JSPS Grant-in-Aid for Scientific Research (B) No.22340052, and by RIKEN 2012 Strategic Programs for R & D.

Appendix A. EOS tables

In this Appendix, we show the concrete values of pressure P and energy density ε as a function of a baryon density $x \equiv \rho/\rho_0$ for H-EOSs, Q-EOSs and interpolated EOSs.

In Table A1, we show H-EOSs with hyperons; TNI2, TNI2u, TNI3, TNI3u [33, 34], AV18+TBF [36] and SCL3 $\Lambda\Sigma$ [39].

Shown in Table A2, NJL Q-EOSs with HK parameter set for various vector interactions $g_v/G_s = 0, 1.0, 1.5$ are listed in each row [43].

In Table A3, interpolated EOSs between TNI2u H-EOS and NJL Q EOS with HK parameter set with $g_v/G_s = 0, 1.0, 1.5$ for $(\bar{\rho}, \Gamma) = (3\rho_0, \rho_0)$ are listed.

Table A1 Pressure $P(\text{MeV}/\text{fm}^3)$ and energy density $\varepsilon(\text{MeV}/\text{fm}^3)$ as a function of a baryon density $x \equiv \rho/\rho_0$ for various hadronic EOSs with hyperons[33, 34, 36, 39].

x	TNI2		TNI3		TNI2u		TNI3u	
	P	ε	P	ε	P	ε	P	ε
1.0	2	162	3	162	2	162	3	162
1.5	7	245	9	246	7	245	9	246
2.0	15	330	20	332	15	330	20	332
2.5	26	418	32	422	26	418	38	422
3.0	40	508	40	513	42	508	61	516
3.5	48	600	48	606	62	601	92	615
4.0	57	693	58	700	87	697	131	718
4.5	67	787	69	795	112	797	174	827
5.0	80	882	82	892	140	899	224	941
5.5	93	979	96	990	173	1005	283	1060
6.0	109	1078	113	1090	211	1113	353	1185
6.5	127	1177	131	1191	255	1226	433	1316
7.0	147	1278	152	1293	304	1341	525	1454
7.5	169	1381	175	1397	360	1461	629	1599
8.0	193	1485	200	1503	422	1584	746	1751
8.5	219	1590	227	1610	492	1712	876	1911
9.0	248	1698	256	1719	568	1843	1020	2079
9.5	278	1807	287	1829	651	1979	1178	2256
10.0	311	1917	321	1942	743	2120	1352	2441

x	Paris+TBF		AV18+TBF		SCL3 $\Lambda\Sigma$		
	P	ε	P	ε	x	P	ε
0.471	0.370	71.2	0.432	71.2	1.02	5.85	167
0.941	2.41	148	2.59	148	1.51	14.6	251
1.18	4.63	187	4.94	187	2.04	28.9	346
1.76	15.5	287	15.5	288	2.51	41.5	434
2.35	31.2	404	29.0	399	3.02	53.5	531
2.94	45.7	503	44.2	505	3.54	67.8	635
3.53	62.3	617	59.9	623	4.07	84.0	740
4.12	79.0	735	75.3	729	4.57	101	841
4.71	99.9	853	94.4	858	5.01	118	933
5.29	117	965	112	970	5.62	144	1063
5.88	145	1128	139	1122	6.02	162	1150
6.47	168	1240	159	1223	6.60	191	1278
7.06	188	1369	181	1341	7.07	216	1384
7.65	213	1470	205	1459	7.58	244	1499
8.24	242	1599	239	1616	8.12	276	1625
8.82	279	1745	270	1745	8.50	300	1715
9.41	307	1874	302	1879	9.11	339	1860
10.0	347	2031	328	1986	9.54	368	1965

Table A2 Pressure $P(\text{MeV}/\text{fm}^3)$ and energy density $\varepsilon(\text{MeV}/\text{fm}^3)$ as a function of a baryon density $x \equiv \rho/\rho_0$ for NJL Q-EOSs with HK parameter set for $g_V = G_S$ [43].

x	$g_V/G_S = 0$		$g_V/G_S = 1$		$g_V/G_S = 1.5$	
	P	ε	P	ε	P	ε
1.0	-0.7633	179.2	8.390	188.3	12.97	192.9
1.5	-1.397	268.1	19.20	288.7	29.49	299.0
2.0	6.721	357.8	43.33	394.5	61.64	412.8
2.5	28.71	451.3	85.91	508.5	114.5	537.1
3.0	58.56	550.0	140.9	632.4	182.1	673.6
3.5	91.96	654.0	204.1	766.2	260.1	822.2
4.0	127.5	762.8	274.0	909.3	347.2	982.5
4.5	158.2	876.1	343.6	1061	436.2	1154
5.0	182.8	992.3	411.6	1221	526.0	1335
5.5	203.0	1111	479.9	1388	618.3	1526
6.0	221.0	1231	550.5	1561	715.2	1725
6.5	238.9	1353	625.6	1740	819.0	1933
7.0	258.3	1476	706.8	1925	931.0	2149
7.5	279.8	1601	794.7	2115	1052	2373
8.0	303.7	1727	889.5	2313	1182	2605
8.5	330.0	1854	991.3	2516	1322	2846
9.0	358.4	1984	1100	2725	1471	3096
9.5	389.9	2114	1215	2941	1628	3354
10	421.3	2247	1337	3163	1794	3620

Table A3 Pressure $P(\text{MeV}/\text{fm}^3)$ and energy density $\varepsilon(\text{MeV}/\text{fm}^3)$ as a function of a baryon density $x \equiv \rho/\rho_0$ for interpolated EOSs between TNI2u H-EOS and NJL Q EOS with HK parameter set with $g_V/G_S = 0, 1.0, 1.5$ for $(\bar{\rho}, \Gamma) = (3\rho_0, \rho_0)$ case. For the practical use, in a hadronic phase, we fit pressure as a function $a\rho^b$ by using the least-squares method.

x	TNI2						TNI2u					
	$g_V/G_S = 0$		$g_V/G_S = 1$		$g_V/G_S = 1.5$		$g_V/G_S = 0$		$g_V/G_S = 1$		$g_V/G_S = 1.5$	
	P	ε	P	ε	P	ε	P	ε	P	ε	P	ε
1.0	2.480	168.9	2.645	179.5	2.727	184.8	2.480	168.8	2.645	179.4	2.727	184.8
1.5	6.737	255.4	7.714	271.5	8.202	279.6	6.737	255.3	7.714	271.4	8.202	279.5
2.0	13.90	343.7	18.26	366.0	20.45	377.1	13.90	343.6	18.26	365.9	20.45	377.0
2.5	26.93	434.4	42.31	464.4	50.00	479.4	26.93	434.3	42.31	464.3	50.00	479.3
3.0	49.03	528.1	90.22	569.3	110.8	589.8	50.19	528.5	91.38	569.7	112.0	590.3
3.5	80.26	629.2	162.2	687.2	203.2	716.2	83.90	627.5	165.8	685.5	206.8	714.5
4.0	119.2	733.0	248.2	814.2	312.7	854.8	122.7	731.6	251.7	812.8	316.2	853.4
4.5	153.9	841.7	330.4	952.0	418.7	1007	156.0	841.7	332.6	952.0	420.9	1007
5.0	181.0	953.8	405.7	1099	518.0	1171	182.1	954.0	406.8	1099	519.1	1171
5.5	202.3	1068	477.3	1252	614.8	1344	202.8	1069	477.8	1253	615.4	1345
6.0	220.7	1185	549.4	1413	713.7	1527	220.9	1185	549.6	1413	714.0	1527
6.5	238.8	1303	625.1	1579	818.3	1718	238.9	1303	625.3	1580	818.4	1718
7.0	258.2	1422	706.6	1752	930.7	1917	258.3	1422	706.6	1752	930.8	1918
7.5	279.8	1543	794.6	1931	1052	2125	279.8	1543	794.6	1931	1052	2125
8.0	303.7	1665	889.5	2115	1182	2341	303.7	1665	889.5	2116	1182	2341
8.5	330.0	1789	991.3	2306	1322	2565	330.0	1789	991.3	2307	1322	2566
9.0	358.4	1914	1100	2503	1471	2798	358.4	1915	1100	2504	1471	2799
9.5	389.0	2041	1215	2707	1628	3039	388.9	2042	1215	2707	1628	3040
10.0	421.3	2170	1337	2916	1794	3289	421.3	2170	1337	2917	1794	3290

References

- [1] K. Fukushima and T. Hatsuda, Rept. Prog. Phys. **74**, 014001 (2011)
- [2] J. M. Lattimer and M. Prakash, Phys. Rept. **442**, 109 (2007)
- [3] As a review, T. Takatsuka, Prog. Theor. Phys. Suppl. **156**, 84 (2004) and references therein.
- [4] S. Weissenborn, D. Chatterjee and J. Schaffner-Bielich, Nucl. Phys. A **881**, 62 (2010)
- [5] H. J. Schulze, A. Polls, A. Ramos and I. Vidana, Phys. Rev. C **73**, 058801 (2006)
- [6] T. Takatsuka, S. Nishizaki and R. Tamagaki, Proc. Int. Symp. "FM50" (AIP Conference proceedings) 209 (2008)
- [7] F. Özel, D. Psaltis, S. Ransom, P. B. Demorest and M. Alford, Astrophys. J. **724**, 1199 (2010)
- [8] H. Djapo, B. J. Schaefer and J. Wambach, Phys. Rev. C **81**, 035803 (2010)
- [9] A. Kurkela, P. Romatschke, A. Vuorinen and B. Wu, arXiv 1006.4062 [astro-ph.HE]
- [10] T. Nagae, Prog. Theor. Phys. Suppl. **185**, 299 (2010)
- [11] H. Tamura, Prog. Theor. Phys. Suppl. **185**, 315 (2010)
- [12] K. Nakazawa and H. Takahashi, Prog. Theor. Phys. Suppl. **185**, 335 (2010)
- [13] T. Inoue *et al.* [HAL QCD Collaboration], Nucl. Phys. A **881**, 28 (2012)
- [14] P. B. Demorest, T. Pennucci, S. M. Ransom, M. S. E. Roberts and J. W. T. Hessels, Nature **467**, 1081 (2010)
- [15] K. Kim, H. K. Lee and M. Rho, Phys. Rev. C **84**, 035810 (2011)
- [16] S. Weissenborn, D. Chatterjee and J. Schaffner-Bielich, arXiv:1112.0234v2 [astro-ph.HE].
- [17] T. Klahn, D. Blaschke and R. Lastowiecki, Acta Phys. Polon. Supp. B **5** 757 (2012)
- [18] S. Weissenborn, I. Sagert, G. Pagliara, M. Hempel and J. Schaffner-Bielich, Astrophys. J. **740**, L14 (2011)
- [19] L. Bonanno and A. Sedrakian, Astron. Astrophys. **539**, A16 (2012)
- [20] H. Chen, M. Baldo, G. F. Burgio and H. J. Schulze, Phys. Rev. D **86**, 045006 (2012)
- [21] S. Schramm, V. Dexheimer, R. Negreiros, T. Schurhoff and J. Steinheimer, arXiv 1202.5113[astro-ph.SR]
- [22] D. L. Whittenbury, J. D. Carroll, A. W. Thomas, K. Tsushima and J. R. Stone, arXiv:1204.2614 [nucl-th]
- [23] T. Katayama, T. Miyatsu and K. Saito, ApJ Supplement Series **203**, 22 (2012)
- [24] T. Takatsuka, T. Hatsuda and K. Masuda, Proceedings of the 11th Int. Symp. on "Origin of Matter and Evolution of Galaxies (OMEG 11)" (Nov.14-17, 2011, RIKEN, Wako, Japan) (2011)
- [25] M. A. Baranov, Phys. Rept. **464**, 71 (2008)
- [26] G. Baym, Physica **96A**, 131 (1979)
- [27] T. Celik, F. Karsch and H. Satz, Phys. Lett. B **97**, 128 (1980)
- [28] T. Schafer and F. Wilczek, Phys. Rev. Lett. **82**, 3956 (1999)
- [29] K. Fukushima, Phys. Lett. B **591**, 277 (2004)
- [30] G. Baym, T. Hatsuda, M. Tachibana and N. Yamamoto, J. Phys. G **35**, 104021 (2008)
- [31] K. Maeda, G. Baym and T. Hatsuda, Phys. Rev. Lett. **103**, 085301 (2009)
- [32] K. Masuda, T. Hatsuda and T. Takatsuka, arXiv 1205.3621[nucl-th] (Astrophys. J. in press)
- [33] S. Nishizaki, Y. Yamamoto and T. Takatsuka, Prog. Theor. Phys. **105**, 607 (2001)
- [34] S. Nishizaki, Y. Yamamoto and T. Takatsuka, Prog. Theor. Phys. **108**, 703 (2002)
- [35] B. Friedman and V.R. Pandharipande, Nucl. Phys. A **361**, 502 (1981)
- [36] M. Baldo, G.F. Burgio and H.J. Schulze, Phys. Rev. C **61**, 055801 (2000)
- [37] Z. H. Li and H.J. Schulze, Phys. Rev. C **78**, 028801 (2008)
- [38] H.J. Schulze and T. Rijken, Phys. Rev. C **84**, 035801 (2011)
- [39] K. Tsubakihara, H. Maekawa, H. Matsumiya and A. Ohnishi, Phys. Rev. C **81**, 065206 (2010)
- [40] A. Akmal, V.R. Pandharipande and D.G. Ravenhall, Phys. Rev. C **58**, 1804 (1998)
- [41] U. Vogel and W. Weise, Prog. Part. Nucl. Phys. **27**, 195 (1991)
- [42] S. P. Klevansky, Rev. Mod. Phys. **64**, 649 (1992)
- [43] T. Hatsuda and T. Kunihiro, Phys. Rep. **247**, 221 (1994)
- [44] M. Buballa, Phys. Rept. **407**, 205 (2005)
- [45] M. Asakawa and K. Yazaki, Nucl. Phys. A **504**, 668 (1989)
- [46] N. M. Bratovic, T. Hatsuda and W. Weise, arXiv:1204.3788 [hep-ph]
- [47] O. Lourenco, M. Dutra, T. Frederico, A. Delfino and M. Malheiro, Phys. Rev. D **85**, 097504 (2012)
- [48] M. Asakawa and T. Hatsuda, Phys. Rev. D **55**, 4488 (1997)
- [49] A. W. Steiner, J. M. Lattimer and E. F. Brown, arXiv:1205.6871 [nucl-th].
- [50] F. Özel, A. Gould and T. Guver, Astrophys. J. **748**, (2012)
- [51] S. Shlomo, V. M. Kolomietz and G. Colò, Eur. Phys. J. A **30**, 23 (2006)
- [52] S. L. Shapiro and S. A. Teukolsky, *Black holes, white dwarfs, and neutron stars: the physics of compact objects*, (John Wiley & Sons, New York, 1983)